Am J Nucl Med Mol Imaging 2013;3(1):16-31
www.ajnmmi.us /ISSN:2160-8407/ajnmmi1207001

Original Article

Utility of 3'-[^{18}F]fluoro-3'-deoxythymidine as a PET tracer to monitor response to gene therapy in a xenograft model of head and neck carcinoma

Neale S Mason[1], Brian J Lopresti[1], James Ruszkiewicz[1], Xinxin Dong[2], Sonali Joyce[3], George Leef[3], Malabika Sen[3], Abdus S Wahed[2], Chester A Mathis[1], Jennifer R Grandis[3,4], Sufi M Thomas[3,4]

[1]Departments of Radiology, [2]Biostatistics, [3]Otolaryngology and [4]Pharmacology and Chemical Biology, University of Pittsburgh and University of Pittsburgh Cancer Institute, Pittsburgh, PA, USA

Received July 10, 2012; Accepted October 2, 2012; Epub January 5, 2013; Published January 15, 2013

Abstract: Noninvasive imaging methodologies are needed to assess treatment responses to novel molecular targeting approaches for the treatment of squamous cell carcinoma of the head and neck (SCCHN). Computer tomography and magnetic resonance imaging do not effectively distinguish tumors from fibrotic tissue commonly associated with SCCHN tumors. Positron emission tomography (PET) offers functional non-invasive imaging of tumors. We determined the uptake of the PET tracers 2-deoxy-2-[^{18}F]fluoro-D-glucose ([^{18}F]FDG) and 3'-[^{18}F]Fluoro-3'-deoxythymidine ([^{18}F]FLT) in several SCCHN xenograft models. In addition, we evaluated the utility of [^{18}F]FLT microPET imaging in monitoring treatment response to an EGFR antisense approach targeted therapy that has shown safety and efficacy in a phase I trial. Two of the 3 SCCHN xenograft models tested demonstrated no appreciable uptake or retention of [^{18}F]FDG, but consistent accumulation of [^{18}F]FLT. The third tumor xenograft SCCHN model (Cal33) demonstrated variable uptake of both tracers. SCCHN xenografts (1483) treated with EGFR antisense gene therapy decreased tumor volumes in 4/6 mice. Reduced uptake of [^{18}F]FLT was observed in tumors that responded to epidermal growth factor antisense (EGFRAS) gene therapy compared to non-responding tumors or tumors treated with control sense plasmid DNA. These findings indicate that [^{18}F]FLT PET imaging may be useful in monitoring SCCHN response to molecular targeted therapies, while [^{18}F]FDG uptake in SCCHN xenografts may not be reflective of the level of metabolic activity characteristic of human SCCHN tumors.

Keywords: Squamous cell carcinoma of the head and neck (SCCHN), positron emission tomography (PET), 2-deoxy-2-[^{18}F]fluoro-D-glucose ([^{18}F]FDG), 3'-[^{18}F]Fluoro-3'-deoxythymidine ([^{18}F]FLT), epidermal growth factor receptor (EGFR), volume of interest (VOI), standardize uptake values (SUV), region of interest (ROI)

Introduction

Squamous cell carcinoma of the head and neck (SCCHN) is the most common malignancy arising in the upper aerodigestive tract. With multimodality treatment (surgery, radiation, and chemotherapy), only 50% of the patients survive their primary tumor. Once the initial tumor is eradicated, patients develop a second primary cancer in the aerodigestive tract at a rate of 5% per year. The complex anatomy of the head and neck region combined with the low sensitivity of physical examination and anatomic imaging modalities [including computer-assisted tomography (CT) or magnetic resonance imaging (MRI)] often obscure the detection of residual or recurrent disease. Prior studies have reported that post-radiation effects cannot be reliably distinguished from post-surgical fibrosis or tumor using CT or MRI [1, 2]. Positron emission tomography (PET) is a non-invasive imaging technique that relies on differential uptake of a radiolabeled molecule or retention of a radiolabeled metabolite that becomes preferentially concentrated in target tissue. The radiotracer 2-deoxy-2-[^{18}F]fluoro-D-glucose ([^{18}F]FDG) is widely used in the clinical management of SCCHN to identify the primary tumor, detect metastases, and evaluate the response of radiation therapy [3].

[^{18}F]FDG PET is avidly taken up by primary and metastatic SCCHN tumors in humans, but may be unable to distinguish persistent SCCHN

tumor from the effects of prior surgical resection and/or radiation therapy [4, 5]. 3'-[^{18}F] Fluoro-3'-deoxythymidine ([^{18}F]FLT) is a PET tracer for which the rate of accumulation may be a useful *in vivo* marker of cellular proliferation rates, and may have an advantage over [^{18}F]FDG PET in the monitoring of SCCHN therapy [6, 7]. While [^{18}F]FDG PET is widely utilized in the clinical management of a variety of cancers, preclinical animal models of many human carcinomas have failed to demonstrate consistent uptake of [^{18}F]FDG in xenografted tumors [8-10]. Two previous studies utilized SCCHN xenograft models and [^{18}F]FDG. In one phosphor imaging-based study that utilized a cell line (LU-HNxSCC-7) which originated from a primary untreated SCCHN tumor, higher levels of [^{18}F]FDG uptake (MBq/g tumor tissue) in hypermetabolism foci were noted. However, this effect was diminished when larger tumor volumes representative of an imaging region of interest (ROI) were examined [11]. The second study utilized the HNX-OE cell line and examined therapy response following radiotherapy demonstrated a decline in tumor to normal tissue measures of [^{18}F]FDG uptake. However, the accumulation of [^{18}F]FDG was characterized as relatively low and considerable variability in FDG uptake was observed before and after radiotherapy in these studies [12]. The present study was undertaken to examine and compare the dynamics of both [^{18}F]FDG and [^{18}F]FLT in preclinical murine models of SCCHN, and determine their utility in evaluating response to molecular targeted strategies in this cancer.

Cumulative evidence suggests that transcriptional activation and gene amplification of the epidermal growth factor receptor (EGFR) leads to over-expression of EGFR mRNA and protein in SCCHN, and EGFR overexpression contributes to tumor progression and adverse outcome [13]. We previously reported a significant inhibition of the growth of SCCHN tumor xenografts treated with EGFR antisense DNA plus liposomes, compared to controls [14]. Toxicity studies demonstrate that adverse effects were restricted to self-limited inflammation at the injection site [15]. Further, we reported that EGFR antisense plasmid DNA is effectively incorporated into HNSCC xenograft tumor tissue [16]. Although we were unable to detect integration of the plasmid DNA, mRNA transcript of the EGFR antisense construct under the U6 promoter was detected in xenograft tumors. A phase I clinical trial was completed using direct intratumoral injection of an EGFR antisense gene in patients with advanced SCCHN achieving a clinical response rate of 29% [17]. Although there was no saline or scrambled control treated patient tumors, EGFR antisense treatment reduced the levels of EGFR compared to baseline levels in treated tumors.

Clinical management can be enhanced by techniques that assess *in vivo* proliferation rates. PET imaging utilizing a suitable radiotracer may represent a non-invasive method of evaluating clinical responses to molecular targeting strategies. In the present study, we evaluated the use of PET imaging in pre-clinical animal models of SCCHN. Since patients with SCCHN tumors demonstrate avid uptake of [^{18}F]FDG in their tumors, we assessed the uptake of [^{18}F]FDG and [^{18}F]FLT in human SCCHN tumors grown as xenografts in athymic nude mice and evaluated the ability of [^{18}F]FLT to monitor SCCHN response to EGFR antisense gene therapy.

Materials and methods

Cell lines and reagents

Human head and neck cancer cell lines 1483 and Cal 33 were maintained in DMEM + 10% fetal bovine serum and OSC19 in MEM+1% non-essential amino acids + 10% fetal bovine serum at 37°C in a 5% CO_2 incubator as described previously [18, 19]. Plasmid DNA pNGVL-1-U6-EGFRAS (antisense) and pNGVL-1-U6-EGFRS (sense) plasmid DNA was amplified in competent DH5a cells (Invitrogen Corporation, Carlsbad, CA) and purified using the Hurricane Maxi Prep kit according to the manufacturer's protocol (Gerard Biotech, Oxford, OH) [14, 16]. Plasmid DNA was suspended in sterile water, the concentration estimated and then diluted to 0.5μg/μl in sterile saline for *in vivo* injections. Antibodies used for immunoblotting of thymidine kinase-1 was obtained from Abcam (Cambridge, MA). Hexokinase-II and β-Actin antibodies were obtained from Cell Signaling Technologies (Danvers, MA), respectively. The EGFR specific antibody was obtained from BD Biosciences (San Jose, CA).

In vivo PET imaging

SCCHN 1483 (one million cells/site) tumors were established subcutaneously on the left and right shoulders (2 tumors/shoulder/mouse) of female athymic nude mice between the ages of 5 and 6 weeks (Harlan Sprague Dawley Inc., Indianapolis, Indiana). PET imaging was performed prior to treatment initiation (pre) and after 3 weeks of treatment (post). Tumors were measured with a vernier caliper in 2 perpendicular dimensions and the volumes were determined as previously described [20]. Animals were initially anesthetized by induction with isoflurane (5%) and maintained on 0.5-1.5% isoflurane in a 60/40 mixture of medical air/oxygen administered by nose cone. Body temperature was maintained throughout the experiment with a thermoelectric heating pad. All animals were allowed free access to food and water prior to the imaging studies and were studied with both [^{18}F]FLT and [^{18}F]FDG. The order of administration ([^{18}F]FDG and [^{18}F]FLT was randomized to preclude any systemic carry-over effect and the second tracer administration and scan session was performed within 24 hours of the initial PET scan session (17-24 hours). Animals were placed in a P4 scanner (Concorde Microsystems, Knoxville, TN) in pairs and injected with 4.81-7.41 MBq of either [^{18}F]FDG or [^{18}F]FLT via the lateral tail vein. The intrinsic volumetric resolution (at the center of the field of view) for the small animal camera used in these studies is 8 mm^3. In initial studies, a 90 min dynamic microPET acquisition was performed following radiotracer injection. In subsequent studies, a static 30 min image was acquired one hour post-injection of the radiotracer. PET emission data were reconstructed using 2-D filtered back projection with a ramp filter. Due to the small mass of the animals, data were not corrected for attenuation or scatter. Volumes of interest (VOI) were defined over 3-4 contiguous planes for each tumor. Standardized uptake values (SUV) were determined using the formula: SUV= (VOI activity x body mass)/ injected activity. Total proliferative volume (TPV) was calculated by multiplying the total tumor volume and mean tumor SUV for each tumor pre- and post-EGFR antisense or sense gene therapy treatment. All procedures were approved by the Institutional Animal Care and Use Committee at the University of Pittsburgh (Protocol Number 1002592A-2).

EGFR antisense gene therapy

Approximately 10^6 SCCHN cells were implanted subcutaneously on the right and left shoulders (2 tumors/mouse) of female nude mice (n=6). When the tumors were established and reached a diameter of 3-4 mm (< 25 mm^3), baseline [^{18}F]FLT and/or [^{18}F]FDG PET images were obtained. Tumor bearing mice were treated with intratumoral injections of plasmid DNA (either EGFR sense or antisense), daily (5 days a week) at 25 μg/tumor (1.25 mg/kg body weight) for 20 days. Since each animal had 2 tumors, one tumor was injected with the EGFR antisense DNA and the other tumor was injected with EGFR sense DNA. Additional PET images were collected post-treatment. PET imaging was performed as described above (*In vivo* PET imaging of SCCHN xenograft tumors). Following imaging, anaesthetized mice were sacrificed by cervical dislocation and tumors were excised.

Immunohistochemistry

Four micron thick sections of paraffin-fixed tumor samples from the EGFR antisense-alone and EGFR sense-alone treatment groups were removed and adhered to slides by heating overnight at 57°C in a dry slide incubator. The specimens were deparaffinized and rehydrated by a series 5 min sequential washes in xylene, ethanol and 95% ethanol. Slides were placed in a 1:10 diluted mixture of methanol/H_2O_2 for 15 min at room temperature and then rinsed two times with distilled water. Antigen retrieval was performed by heating uncovered slides in boiling citrate buffer for ten min. Slides were allowed to cool at room temperature for one hour and blocked in PBS/Tween buffer for 25 min at room temperature. The blocking solution was drained and slides incubated in monoclonal Ki-67 primary antibody at room temperature for one hour. The antibody is well suited to detection of the 345 and 395 kD isoforms of Ki-67 in paraffin embedded tissue. Slides were rinsed with phosphate buffered saline (PBS)/Tween® for five min. Secondary antibody was added in dilution ratio of 1:2000 and slides incubated in a humidified chamber for 30 min at room temperature. Slides were rinsed with PBS/Tween® for five min and incubated in avidin-biotin complex (ABC) for 30 min in a humidified chamber. Afterwards, the slides were then rinsed again in PBS/Tween® for 5 min, incubated in diaminobenzidine (DAB) for 5-10 min

Table 1. Standardized Uptake Values (SUV) of [^{18}F]FLT and [^{18}F]FDG at baseline in SCCHN tumor-bearing mice averaged over 60-90 min post-injection

		[^{18}F]FLT		[^{18}F]FDG	
Cell Line	*n**	Mean (SD)	range	Mean (SD)	range
1483	6	2.18 (0.39)	1.83 - 2.87	0.97 (0.08)	0.89 - 1.04
OSC19	4	1.36 (0.28)	1.10 - 1.72	1.07 (0.10)	0.93 - 1.15
Cal 33	16	1.31 (0.26)	1.03 - 2.02	0.99 (0.08)	0.81 - 1.10

**n* refers to the number of tumors included in the average (multiple tumors per animal).

and rinsed with distilled water. Slides were counterstained in Shandon Hematoxylin for 3 minutes, rinsed with distilled water, PBS, xylene, various concentrations of ethanol and cover-slipped. A dark brown staining of the nuclei indicated positive Ki-67 staining. The cells with dark brown nuclei were counted under 200X magnification by 2 individuals who were blinded to the treatment groups. Positive cells in 4-5 separate fields were counted for each slide.

Assessment [^{18}F]FLT uptake and metabolism in SCCHN xenografts

Athymic nude mice with SCCHN xenografts (Cal 33) were administered a bolus injection of 4.81-7.41 MBq of [^{18}F]FLT via the lateral tail vein. The animals were sacrificed ninety minutes post-injection by cervical dislocation and tumors were excised. Plasma and tumor samples were analyzed for the presence of [^{18}F]FLT metabolites using reverse-phase HPLC utilizing a modification of previously reported methods [21]. Plasma samples were deproteinated with ice-cold acetonitrile (2 x volume of plasma) followed by centrifugation at 4˚C (3000 x g, 5 min). The resultant supernatant was concentrated under a stream of nitrogen at 4˚C, suspended in HPLC mobile phase and filtered using a 0.2 micron filter prior to HPLC analysis. Samples of tumor were cut into small pieces and homogenized (Polytron PT1200-c) with ice-cold acetonitrile. The tissue homogenate was then centrifuged at 4˚C (3000 x g, 5 min). The resultant supernatant was then treated in a manner identical to the plasma samples. The analytical HPLC system consisted of a Phenomenex Prodigy ODS-3 5 micron (4.6 x 250 mm) column eluted with 10% ethanol/phosphate buffered saline at a flow of 1.5 mL/min. The percentages of unmetabolized [^{18}F]FLT and phosphorylated metabolite (5'-monophosphorylated analog) were determined by the integration of radioactive peaks detected using a flow-through HPLC NaI detector (Raytest GABI system).

Statistical analyses

The total tumor volume, standardized uptake values (SUV) and total proliferative volume (TPV) are summarized using descriptive statistics and their post-treatment evolution over time are shown graphically using line plots. Post-treatment changes (at week 20) were compared between the EGFR antisense- and EGFR sense-treated tumors using paired exact Wilcoxon sign rank tests. The rate of change in total volume over time between the two groups determine by fitting a linear model using generalized estimating equations. All analyses were conducted using R programming language [22].

Results

[^{18}F]FLT, but not [^{18}F]FDG, is taken up by SCCHN xenografts

Since the majority of human SCCHN tumors demonstrate avid [^{18}F]FDG uptake, we hypothesized that cell lines derived from SCCHN patient tumors should similarly demonstrate incorporation of [^{18}F]FDG in xenografts. In addition, we hypothesized that xenograft tumors derived from SCCHN cell lines may be imaged successfully using the radiolabeled thymidine analogue [^{18}F]FLT. Surprisingly, the SUVs of [^{18}F]FDG in the 1483 (mean ± SD = 0.97 ± 0.08), OSC 19 (1.07 ± 0.10) or Cal 33 (0.99 ± 0.08) SCCHN cell lines are all approximately 1 and thus do not indicate any selective localization of [^{18}F]FDG in the SCCHN xenografts (**Table 1**). Uptake of [^{18}F]FDG was greatest in the heart and brain and elevated in other peripheral tissues. In contrast, time-activity curves following [^{18}F]FLT injection show consistent accumulation in 1483, OSC19 and Cal 33 tumors, negligible uptake in brain, and an otherwise uniform

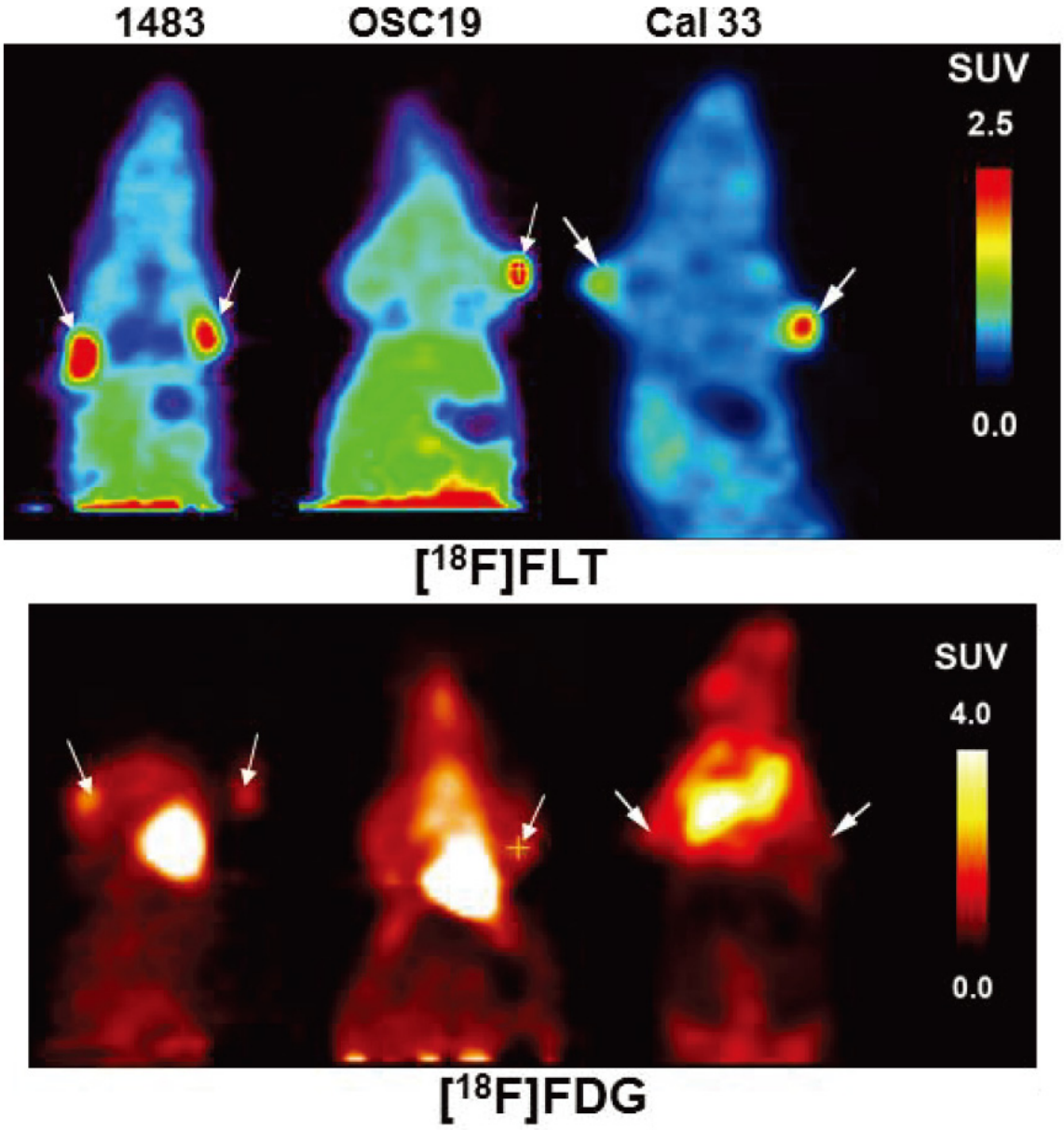

Figure 1. microPET imaging of SCCHN tumor xenografts demonstrate uptake of [^{18}F]FLT and [^{18}F]FDG. Representative summed microPET images taken 40-90 min, post-injection of radiotracer in mice bearing 1483, OSC19 or Cal 33 tumors with arrows indicating the location of the tumor. The uptake was assessed 2-3 times with each tumor type.

distribution. Enhanced [^{18}F]FLT uptake, indicated by an SUV greater than 1, SUV was observed in 1483 (2.18 ± 0.39; range: 1.8 - 2.8), OSC 19 (1.36 ± 0.28; range: 1.1 – 1.72) and Cal 33 (1.31 ± 0.26; range 1.03-2.02) cells (**Table 1**). While the SCCHN cell lines examined were not generally [^{18}F]FDG avid, all of the SCCHN cell lines examined in this work demonstrated tumor uptake of [^{18}F]FLT (**Figure 1**). Thus, the cell lines tested were imaged with [^{18}F]FLT in subsequent studies.

Hexokinase II and thymidine kinase-1 levels in SCCHN cell lines do not correlate with uptake of [^{18}F]FDG or [^{18}F]FLT

In general, [^{18}F]FDG accumulates in tissues with high glycolytic activity while [^{18}F]FLT accumulates in proliferating cells. Tumor uptake of [^{18}F]FLT occurs via both passive and facilitated transport by sodium dependent carriers [23]. [^{18}F]FDG enters the cells via the glucose transporters GLUT-1 and GLUT-3 located on the cell

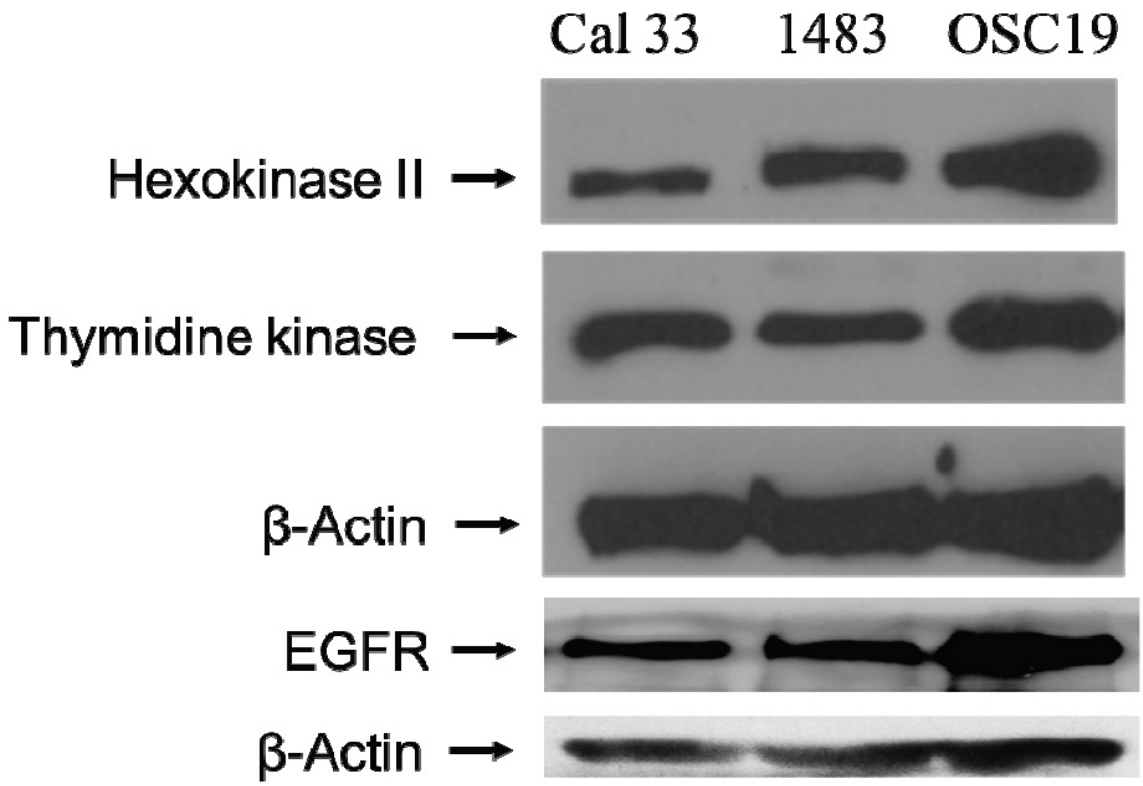

Figure 2. SCCHN cell lines express hexokinase II and thymidine kinase. SCCHN cell lines 1483, OSC19 and Cal 33 were lysed and the proteins were fractionated on an 8% PAGE. Immunoblotting was carried out and the levels of hexokinase, thymidine kinase and EGFR were determined in the three cell lines. β-Actin levels demonstrate equal loading of protein in all lanes. The experiment was repeated twice with similar results.

membrane [24]. Once inside the cell, both tracers are phosphorylated ([^{18}F]FDG by hexokinase and [^{18}F]FLT by thymidine kinase) rendering them essentially cell membrane impermeable and trapping the radioactivity inside the cells. Levels of hexokinase II and thymidine kinase proteins have been reported to correlate with enzyme activity [25, 26]. In most cases, the concentration of phosphorylated tracers within carcinoma cells increases with time and plateaus approximately 90 minutes post-tracer administration. In order to determine the levels of these key enzymes (hexokinase II and thymidine kinase) in SCCHN cells, we carried out immunoblotting analyses of SCCHN cell lysates from the cell lines examined (1483, OSC19, and Cal 33). In these studies, while these SCCHN cell lines demonstrated hexokinase II expression (**Figure 2**), none of the cell lines were consistently [^{18}F]FDG avid (**Figure 1**). In addition, levels of thymidine kinase-1 were examined and found to not correspond with uptake of [^{18}F]FLT in these SCCHN xenografts (**Figure 1** and **2**). We examined the levels of EGFR across Cal33, 1483 and OSC19. All 3 lines expressed EGFR protein (**Figure 2**).

Effect of EGFR antisense gene therapy on SCCHN xenograft growth and proliferation

Previous reports in human lung tumors demonstrate a correlation between increased tumor growth and uptake of [^{18}F]FLT [27, 28]. Inhibition of the EGFR signaling axis in preclinical models has been previously reported to reduce survival, tumor cell proliferation and increase apoptosis in tumors [29]. We previously demonstrated that liposome-mediated delivery of EGFR antisense gene reduces SCCHN xenograft tumor growth [14, 30]. Further, EGFR antisense effectively reduced EGFR levels in tumors. Since the EGFR antisense gene was administered without lipids in the phase I clinical trial, we assessed the antitumor efficacy of EGFR antisense plasmid DNA when administered via intratumoral injections without a lipid carrier in our xenograft model. The purpose of these

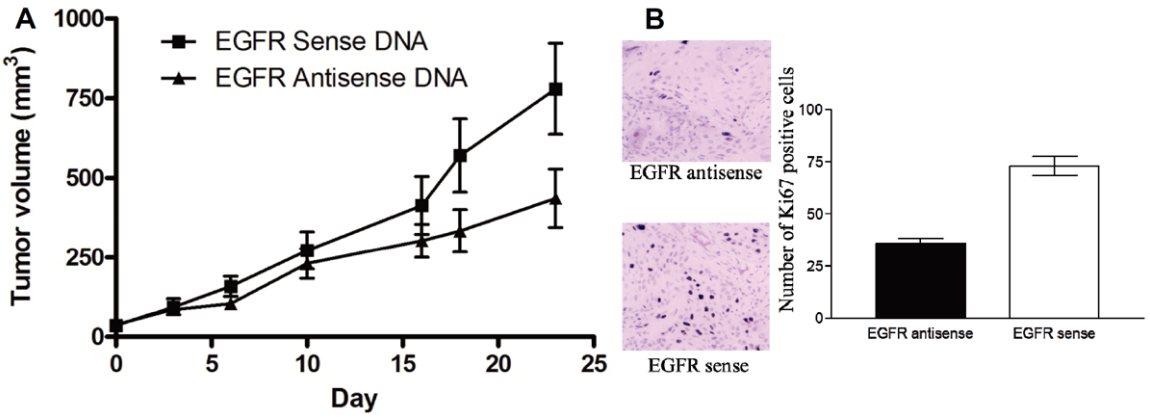

Figure 3. Intratumoral administration of EGFR antisense plasmid DNA has antitumor efficacy. One million SCCHN cells (1483) were injected subcutaneously into six athymic nude mice on both flanks. EGFR sense plasmid DNA (■) or antisense plasmid DNA (▲) (25 μg/tumor) was administered daily into the left and right tumor respectively. Tumors were measured twice a week. The graph depicts growth of the tumors over the treatment period. B: EGFR antisense gene therapy reduces SCCHN xenograft cell proliferation. SCCHN tumors treated with either EGFR antisense or sense gene therapy were paraffin-embedded and examined for proliferation using Ki-67 staining. Positive cells demonstrated by the dark brown nuclear staining were counted under 400X magnification in 10 separate fields. There was a significant difference between tumors treated with EGFR antisense oligonucleotides compared to the control (p= 0.0001). Error bars indicate ± SEM.

studies was to determine if PET imaging could be used to monitor response to EGFR antisense gene therapy. Intratumoral administration of EGFR antisense gene therapy reduced growth in 4 of 6 SCCHN xenograft tumors in the absence of a liposome carrier (**Figure 3A**). The overall antisense treated tumor volumes were not significantly different from sense-treated tumor volumes of the opposite flank (day 20 signed rank P = 0.22). However, there was a significant reduction in the rate of tumor growth in mice treated with the EGFR antisense sense (approximately 22 mm^3 per day) compared with EGFR sense control (approximately 41 mm^3 per day) treated tumors (P=0.03).

Previous reports in human lung tumors demonstrate a correlation between increased expression of Ki-67 and uptake of [^{18}F]FLT [25, 26]. Inhibition of the EGFR signaling axis in preclinical models has been previously reported to reduce survival, tumor cell proliferation and increase apoptosis in tumors [27]. In this study we examined xenograft tumor cell proliferation in EGFR antisense DNA injected intratumorally without a lipid carrier. As shown in **Figure 3B**, tumors treated with EGFR antisense plasmid DNA demonstrated fewer Ki-67 positive cells compared to tumors administered the EGFR sense control plasmid DNA (p=0.0001).

[^{18}F]FLT PET imaging correlates with response to EGFR antisense gene therapy

Previous studies have reported reduced uptake of [^{18}F]FLT in tumors as early as 24 h post-treatment, before changes in tumor volume become apparent [31, 32]. In order to assess early changes in SCCHN proliferation, we assessed [^{18}F]FLT uptake in SCCHN xenograft tumors three days post-treatment and at the end of the study (20 days of treatment). EGFR antisense gene therapy compared to the sense control did not reduce the tumor volumes of mice after 3 days of treatment (data not shown). Since each mouse was implanted with two tumors (one treated with EGFR antisense gene therapy and the second with EGFR sense control plasmid), post-treatment changes in the ratio of the total proliferative volume (TPV = total tumor volume X mean tumor SUV) and total tumor volume between the EGFR antisense (treated) and EGFR sense (control) tumors within an animal are indicative of the treatment effects of the EGFR antisense gene therapy (**Table 2**). In the 1483 xenograft model, a decrease in median tumor volume was achieved in 4 of 6 tumors treated with the EGFR antisense plasmid compared to EGFR sense control treatment over a 20-day treatment regimen (P=0.22). Throughout the course of the experiment,

Table 2. Tumor volume and TPV values for each animal post treatment

Animal ID	Tumor Volume (mm^3)		TPV	
	Sense	Anitsense	Sense	Anitsense
A1	509.012	312.666	414.85	206.05
A2	769.147	320.0	626.86	210.88
A3	1400.773	196.520	1147.3	128.91
B1	651.301	669.272	530.82	441.05
B2	435.938	759.027	358.55	500.19
B5	912.384	359.528	743.59	237.19

increases in tumor volumes ranging from 8 to 71 times the initial tumor volume were observed for EGFR sense control tumors. By comparison, the EGFR antisense treated tumor volumes increased over the course of the study by only 2.5-12.9 times the initial tumor volumes. In 2/6 animals (B1 and B2), there was an increase in the volume of EGFR antisense treated tumor when compared to the corresponding sense control tumor (**Figure 4A**). Thus, the TPV ratio of EGFR antisense versus EGFR sense treated tumors was below 1 in 4 responder mice and above 1 in 2 non-responder mice post-treatment (**Figure 4B**). A decrease in TPV was observed in 5 of 6 tumors treated with the EGFR antisense plasmid compared to EGFR sense control treatment (P=0.09) and the mean (SD) TPV ratio between the EGFR antisense treated tumors and EGFR sense control treated and tumors was 1.24 (0.64) in the initial pre-treatment evaluation and 0.58 (0.46) in the post-treatment evaluation. This decrease in the average TPV ratio represents an increase in the total proliferative volume in the sense control treated tumors when compared to the antisense treated tumors (**Figure 4B**). Animals (B1 and B2) that did not respond to treatment demonstrate higher TPV ratios post-treatment, indicating a positive correlation between tumor size (volume) and uptake of the tracer. Thus, [^{18}F]FLT PET imaging accurately measured the response to treatment.

[^{18}F]FLT metabolite is retained in SCCHN xenografts

Analysis of rodent plasma samples demonstrated that >98% of the radioactivity present in the blood corresponded to intact [^{18}F]FLT (data not shown), in accordance with previously published data [21]. Approximately 40% of the radioactivity in the xenograft tumor was recovered following homogenization, deproteination and filtration prior to HPLC. The analytical HPLC analyses demonstrated that 40-60% of the radioactivity that was extracted from the tumors was in the form of the 5'-monophosphorylated analog of [^{18}F]FLT. While these results are qualitative in nature (owing to the inefficiency of the tumor extraction and partial recovery of activity upon redissolving in HPLC mobile phase prior to analysis), they do demonstrate [^{18}F]FLT metabolism in these xenografts.

Discussion

The most commonly utilized parameter in clinical [^{18}F]FDG PET studies is the standardized uptake value (SUV). Recently, the use of overall tumor volume (TV) has been explored as a more sensitive index for prognosis and therapy response assessment [33, 34]. Other outcome measures for these types of studies have been explored including total glycolytic volume (TGV) and total proliferative volume (TPV) (for [^{18}F]FDG and [^{18}F]FLT, respectively), which are defined as the product of total tumor volume and mean tumor SUV [33]. [^{18}F]FDG uptake has been previously reported in several tumor types including SCCHN [35], and has been useful for locoregional staging of SCCHN as well as for detection of distant of synchronous second primary tumors [36, 37]. Several factors affecting [^{18}F]FDG uptake in SCCHN tumors include the presence of hypoxic regions within the tumor and the tumor grade [38]. The effect of hypoxia on the accumulation of tracers utilized in this study ([^{18}F]FDG and [^{18}F]FLT) is not completely clear. Some *in vitro* studies would indicate that the uptake of FDG increases in hypoxic tumor cells (whether via increased membrane transport or the impact of enhanced FDG phosphorylation) [39]. Another study of single-dose radiotherapy effects in human squamous cell carcinoma xenograft claims that [^{18}F]FDG

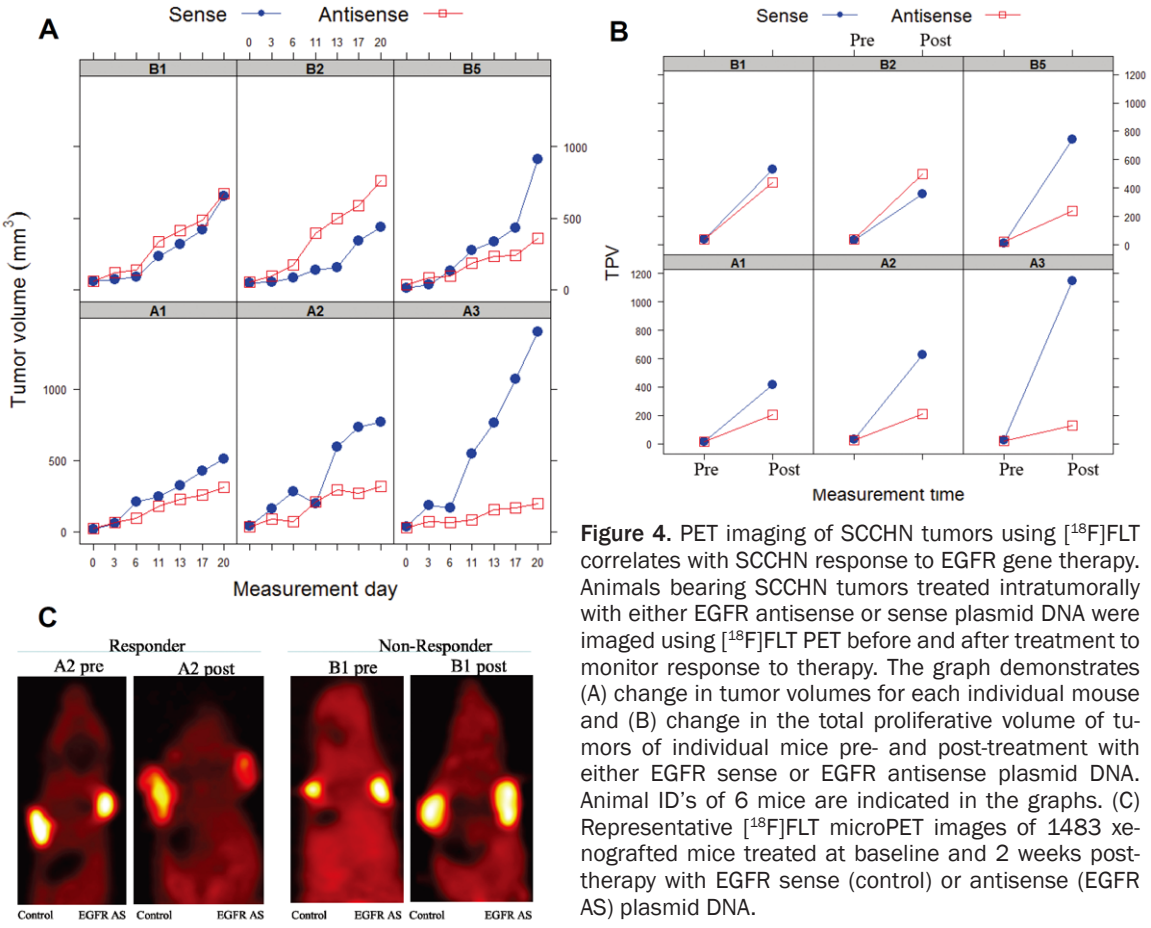

Figure 4. PET imaging of SCCHN tumors using [^{18}F]FLT correlates with SCCHN response to EGFR gene therapy. Animals bearing SCCHN tumors treated intratumorally with either EGFR antisense or sense plasmid DNA were imaged using [^{18}F]FLT PET before and after treatment to monitor response to therapy. The graph demonstrates (A) change in tumor volumes for each individual mouse and (B) change in the total proliferative volume of tumors of individual mice pre- and post-treatment with either EGFR sense or EGFR antisense plasmid DNA. Animal ID's of 6 mice are indicated in the graphs. (C) Representative [^{18}F]FLT microPET images of 1483 xenografted mice treated at baseline and 2 weeks post-therapy with EGFR sense (control) or antisense (EGFR AS) plasmid DNA.

uptake is constant in tumor necrosis over time, while uptake of [^{18}F]FDG decreased in vital tumor area and particularly in hypoxic regions. This study demonstrated no differences in [^{18}F]FDG uptake between area of tumors that are or are not stained with Ki-67 or with BrdU and the authors claimed that SUVmax does not necessarily reflect changes in tumor biology after irradiation [40]. *Ex vivo* autoradiography studies in a rodent model of cancer demonstrated good correlation between areas of hypoxia (as evidenced by [^{18}F]FMISO and [Cu-64]ATSM uptake) and areas of proliferation ([^{18}F]FLT. However, the correlation between areas of glucose utilization ([^{18}F]FDG) and hypoxia ([Cu-64]ATSM) was very poor [41]. In patients with non-small-cell lung cancer, a small study demonstrated a weak correlation between uptake associated with proliferation ([^{18}F]FLT) and uptake associated with hypoxia ([^{18}F]FMISO) [42].

[^{18}F]FDG PET imaging has also been used in the clinical management of SCCHN to identify the primary tumor and evaluate the response to radiation therapy [43]. In this study we examined the uptake of [^{18}F]FDG in three SCCHN xenograft models and demonstrated that although these preclinical models express hexokinase II, there was no appreciable uptake of [^{18}F]FDG in the xenografted tumors. A possible explanation for the lack of significant uptake of [^{18}F]FDG by these SCCHN xenografts may be related to blood glucose levels in these animals at the time of the scan. In one study fasting for 8-12 hours prior to administration of [^{18}F]FDG led to significantly higher tumor uptake in a xenograft model (4-fold) when compared to animals with free access to food [44]. However, there are conflicting reports regarding the correlation between fasting and [^{18}F]FDG uptake in animal models of cancer. Dandekar, *et al.* demonstrated reasonable reproducibility in serial FDG scans performed 6 hours apart in mouse tumor xenografts B16F10 murine melanoma even though there was a significant difference in mean blood glucose levels (91.3 ± 25.3 mg/dL vs. 58.1 ± 20.1 mg/dL) between the two serial scans [45]. Serial [^{18}F]FDG scans (6 h

apart) in C6 rat glioma xenografts also demonstrated reasonable reproducibility [44]. However, we were unable to detect significant [^{18}F]FDG uptake in the SCCHN xenografts tested in animals without fasting and animals fasted for 8 h (data not shown). Reports suggest that several SCCHN cell lines, including SCC-4, HNX-OE, FaDu and Cal27, utilized in animal models incorporate [^{18}F]FDG [12, 46, 47]. While SCCHN patients are routinely evaluated using [^{18}F]FDG, it would seem that only certain SCCHN lines can be imaged using [^{18}F]FDG successfully when implanted into immunodeficient mice.

[^{18}F]FLT is a PET radiotracer that has been utilized to image various tumor types including lung carcinoma [48]. Although [^{18}F]FLT accumulation in the tumor occurs following phosphorylation by thymidine kinase-1 (TK-1), TK-1 activity does not correlate directly with tumor cell proliferation since [^{18}F]FLT uptake is 3-4 times higher in malignant cells than in proliferating benign cells [49]. Previous reports demonstrated the incorporation of phosphorylated FLT into DNA [49, 50]. Recently, attenuation of [^{18}F]FLT uptake on TK-1 siRNA treatment in SCCHN was reported in A431 cells and in the SCCHN cell line SCC1 [51]. A variety of issues arise that complicate the interpretation of these data. The contribution of partial volume effects in these relatively small tumors (especially at baseline), as well as the inability to assess the potential contribution of infiltration of the administered doses and thus accurately determine the SUV measures, contribute to variability in the PET SUV outcome measures. A major limitation of small animal PET imaging studies, particularly in mice imaging studies, is the underestimation of the true radioactivity concentration due to partial volume blurring. This effect arises as a consequence of the limited volume resolution of PET detectors. As illustrated by Mannheim and colleagues [52], the recovery of radioactivity from small image features (< 5 mm diameter), may be 20% or lower using a high-resolution preclinical PET scanner, depending on the contrast ratio between the feature to background. A recovery of 20% would result in a 5-fold underestimation of SUV. SUV's of 1 or even less than 1 are not uncommon in mouse studies [53, 54]. Additional confounders in the interpretation of this data relate to the varying amounts of necrosis present in the tumors at the time of analysis and the relatively small number of animals utilized for the longitudinal studies. However, we were able to demonstrate a positive trend in overall proliferative status (as measured by total proliferative volume) in xenograft tumor models following EGFR antisense therapy. Our data corroborate these findings showing reduced [^{18}F]FLT uptake in tumors with fewer proliferating cells. It should be noted that this difference is driven by both changes in total tumor volume and [^{18}F]FLT SUV. The mean SUV ratio in the antisense treated tumors measured pre- and post-treatment was 1.04 +/-0.21, denoting no significant change in SUV value.

Several studies reported that targeting EGFR in SCCHN reduces proliferation [14, 55]. In a recently concluded phase I trial, antisense gene therapy targeting EGFR was well tolerated in SCCHN patients [17]. Further, a 29% clinical response was observed after EGFR antisense gene therapy with reduced uptake of [^{18}F]FDG in SCCHN patients. Previous reports demonstrate that EGFR levels determined by immunohistochemistry do not predict responsiveness to EGFR targeted therapies [56]. However, the degree of EGFR downregulation post treatment is a predictor of treatment response [17]. In this study, we examined the efficacy of PET in monitoring response to EGFR antisense gene therapy in animal models. Our data demonstrate that [^{18}F]FLT preferentially localizes to SCCHN xenograft tumors and the uptake is attenuated in tumors that respond to EGFR antisense treatment. In a recent report, treatment of SCCHN xenograft tumors with either a small molecule EGFR inhibitor or an anti-EGFR therapeutic antibody reduced [^{18}F]FLT uptake as early as 72 h after the initiation of treatment [51]. Small molecule inhibitors and anti-EGFR antibodies prevent receptor activation and thus elicit rapid antitumor effects. However, clinical trials demonstrate relatively low clinical response rates (5-15%) to single agent small molecule inhibitors or anti-EGFR antibodies in recurrent/metastatic SCCHN [57, 58]. Targeting EGFR by reducing its total protein levels as opposed to blocking EGFR tyrosine kinase activity may be an improved approach to overcome resistance to existing EGFR inhibitors.

While [^{18}F]FDG is widely utilized in clinical oncology applications, we were unable to consistently detect uptake of [^{18}F]FDG in our model systems. This discrepancy points to a potential

Table 3. Reports in literature pertaining to uptake of [^{18}F]FLT and/or [^{18}F]FDG in xenograft tumor models

Xenograft model	[^{18}F]FDG uptake	[^{18}F]FLT uptake	References
LNCAP (prostate cancer)	-	Not studied	[67]
CWR22 (prostate cancer)	+	Not studied	[68]
RH-30 (rhabdomyosarcoma)	+	Not studied	[69]
GBM (glioblastoma)	-	-	[70]
HNX-OE (SCCHN)	+	+	[12]
SKMEL-28 (melanoma)	Not studied	+	[71]
U87 MG (glioblastoma)	+	Not studied	[72]
Panc420 (pancreatic cancer)	-	Not studied	[73]
Panc 194 (pancreatic cancer)	+/-	Not studied	[73]
Panc 140 (pancreatic cancer)	-	Not studied	[73]
Panc 1 (pancreatic cancer)	+/-	Not studied	[73]
BxPC 3 (pancreatic cancer)	+/-	+	[73, 74]
BT474 (breast carcinoma)	-	-	[75]
HCT116 (colorectal carcinoma)	+	+	[76, 77]
HCA7 (colorectal carcinoma)	+	+	[76]
Daudi (B-cell lymphoma)	+	+	[78]
GIST (gastrointestinal stromal tumor)	+	Not studied	[79]
E98 DIPG (glioma)	Not studied	-	[80]
SK-N-SH (neuroblastoma)	-	+	[81]
PancTul (pancreatic cancer)	Low uptake	+	[74]
Colo357	Low uptake	+	[74]
H586 (lung cancer)	+	+	[77]
KB31 (cervical cancer)	+	+	[77]
MDA-MB-435 (breast cancer)	+	Not studied	[82]

limitation of murine xenograft models with respect to non-invasive PET imaging and [^{18}F]FDG and supports the use of direct human studies when [^{18}F]FDG imaging is to be used as an endpoint. [^{18}F]FLT PET imaging provides important information on proliferation that may prove beneficial in the utilization of PET imaging in clinical applications. The ability of [^{18}F]FLT PET imaging to provide information regarding the efficacy of EGFR antisense gene therapy in xenograft SCCHN tumor models illustrates the potential utility of this imaging application. Another application of PET imaging involves EGFR-directed tracers that could be used to measure the levels of EGFR being expressed in tumors. Radiolabeled anti-EGFR antibodies directed against EGFR are currently being tested in preclinical models [59-61]. Future studies could incorporate this biologic imaging strategy to identify possible responders and monitor response to EGFR-targeted therapies with [^{18}F]FLT PET imaging.

A review of published reports that utilized either [^{18}F]FDG or [^{18}F]FLT in preclinical murine models of cancer demonstrate a large variability in utility of non-invasive PET imaging in these types of models (**Table 3**). In approximately twenty xenograft tumor models and six orthotopic murine tumor models where [^{18}F]FDG was utilized in a preclinical imaging paradigm, [^{18}F]FDG uptake was either not visible or the imaging results were not indicative of therapy response in 15 of these models (62%). The number of models that utilized [^{18}F]FLT in a preclinical imaging paradigm were smaller (13 studies) and here the number of studies where [^{18}F]FLT uptake was either not visible of not

indicative of therapy response was still a relatively high percentage (46%). These results as well as the inability to consistently visualize [^{18}F]FDG uptake in the xenograft model(s) we examined point to the necessity to individually qualify murine xenograft tumor models as useful in preclinical imaging paradigms that utilize molecular imaging tracers such as [^{18}F]FDG or [^{18}F]FLT. Whether these failures of non-invasive imaging studies in these xenograft models are a result of tumor perfusion, transport or phosphorylation enzyme levels or activity in murine models, partial volume effects, animal handling issues or some combination of all of these are unclear. While a few studies have provided direct comparisons of [^{18}F]FDG and [^{18}F]FLT in lung cancer [62, 63] and esophageal cancer [64, 65], there is much less information on the comparative utility of these two PET tracers in primary head and neck cancer in the clinical setting [66]. The results of the present study suggests that larger direct comparison clinical trials are needed to assess the comparative utility of [^{18}F]FDG and [^{18}F]FLT in human head and neck cancer.

Funding

This work was supported by NIH grants R21 CA096815, P50 CA097190, and the American Cancer Society (to JRG).

Address correspondence to: Dr. Sufi Mary Thomas, University of Pittsburgh, 200 Lothrop Street, W947 BST, Pittsburgh, PA 15213, USA. Tel: +1-412-3835403; Fax: +1-412-3835409; E-mail: smt30@pitt.edu

References

[1] Anzai Y, Carroll WR, Quint DJ, Bradford CR, Minoshima S, Wolf GT and Wahl RL. Recurrence of head and neck cancer after surgery or irradiation: prospective comparison of 2-deoxy-2-[F-18]fluoro-D-glucose PET and MR imaging diagnoses. Radiology 1996; 200: 135-141.

[2] Greven KM, Williams DW 3rd, Keyes JW Jr, McGuirt WF, Watson NE Jr, Randall ME, Raben M, Geisinger KR and Cappellari JO. Positron emission tomography of patients with head and neck carcinoma before and after high dose irradiation. Cancer 1994; 74: 1355-1359.

[3] Dobert N, Kovacs AF, Menzel C, Hamscho N, Yuen Yuen H, Engels K, Walendzik H and Grunwald F. The prognostic value of FDG PET in head and neck cancer. Correlation with histopathology. Q J Nucl Med Mol Imaging 2005; 49: 253-257.

[4] Nam SY, Lee SW, Im KC, Kim JS, Kim SY, Choi SH, Ryu JS, Moon DH, Oh SJ, Yi BY, Kim JH, Ahn SD, Shin SS, Kim SB, Choi EK and Lee BJ. Early evaluation of the response to radiotherapy of patients with squamous cell carcinoma of the head and neck using ^{18}FDG-PET. Oral Oncol 2005; 41: 390-395.

[5] Kim SY, Lee SW, Nam SY, Im KC, Kim JS, Oh SJ, Ahn SD, Shin SS, Choi EK and Kim JH. The Feasibility of ^{18}F-FDG PET scans 1 month after completing radiotherapy of squamous cell carcinoma of the head and neck. J Nucl Med 2007; 48: 373-378.

[6] Shields AF, Grierson JR, Dohmen BM, Machulla HJ, Stayanoff JC, Lawhorn-Crews JM, Obradovich JE, Muzik O and Mangner TJ. Imaging proliferation in vivo with [F-18]FLT and positron emission tomography. Nat Med 1998; 4: 1334-1336.

[7] Garcia C and Flamen P. Role of positron emission tomography in the management of head and neck cancer in the molecular therapy era. Curr Opin Oncol 2008; 20: 275-279.

[8] Wagner M, Seitz U, Buck A, Neumaier B, Schultheiss S, Bangerter M, Bommer M, Leithauser F, Wawra E, Munzert G and Reske SN. 3'-[^{18}F]fluoro-3'-deoxythymidine ([^{18}F]-FLT) as positron emission tomography tracer for imaging proliferation in a murine B-Cell lymphoma model and in the human disease. Cancer Res 2003; 63: 2681-2687.

[9] Oyama N, Kim J, Jones LA, Mercer NM, Engelbach JA, Sharp TL and Welch MJ. MicroPET assessment of androgenic control of glucose and acetate uptake in the rat prostate and a prostate cancer tumor model. Nucl Med Biol 2002; 29: 783-790.

[10] Tatsumi M, Nakamoto Y, Traughber B, Marshall LT, Geschwind JF and Wahl RL. Initial experience in small animal tumor imaging with a clinical positron emission tomography/computed tomography scanner using 2-[F-18]fluoro-2-deoxy-D-glucose. Cancer Res 2003; 63: 6252-6257.

[11] Bjurberg M, Henriksson E, Brun E, Ekblad L, Ohlsson T, Brun A and Kjellen E. Early changes in 2-deoxy-2-[^{18}F]fluoro-D-glucose metabolism in squamous-cell carcinoma during chemotherapy in vivo and in vitro. Cancer Biother Radiopharm 2009; 24: 327-332.

[12] Molthoff CF, Klabbers BM, Berkhof J, Felten JT, van Gelder M, Windhorst AD, Slotman BJ and Lammertsma AA. Monitoring response to radiotherapy in human squamous cell cancer bearing nude mice: comparison of 2'-deoxy-2'-[^{18}F]fluoro-D-glucose (FDG) and 3'-[^{18}F]fluo-

ro-3'-deoxythymidine (FLT). Mol Imaging Biol 2007; 9: 340-347.
[13] Grandis JR, Melhem MF, Barnes EL and Tweardy DJ. Quantitative immunohistochemical analysis of transforming growth factor- alpha and epidermal growth factor receptor in patients with squamous cell carcinoma of the head and neck. Cancer 1996; 78: 1284-1292.
[14] He Y, Zeng Q, Drenning SD, Melhem MF, Tweardy DJ, Huang L and Grandis JR. Inhibition of human squamous cell carcinoma growth in vivo by epidermal growth factor receptor antisense RNA transcribed from the U6 promoter. J Natl Cancer Inst 1998; 90: 1080-1087.
[15] Zeng Q, Dhir R, Kanter P, Huang L and Rubin Grandis J. Lack of toxicity of EGFR antisense gene therapy. J Exp Ther and Oncology 2002; 2: 174-186.
[16] Thomas SM, Zeng Q, Dyer KF, Suscovich TJ, Kanter PM, Whalen JD, Watkins SF and Grandis JR. Tissue distribution of liposome-mediated epidermal growth factor receptor antisense gene therapy. Cancer Gene Ther 2003; 10: 518-528.
[17] Lai SY, Koppikar P, Thomas SM, Childs EE, Egloff AM, Seethala RR, Branstetter BF, Gooding WE, Muthukrishnan A, Mountz JM, Lui VW, Shin DM, Agarwala SS, Johnson R, Couture LA, Myers EN, Johnson JT, Mills G, Argiris A and Grandis JR. Intratumoral epidermal growth factor receptor antisense DNA therapy in head and neck cancer: first human application and potential antitumor mechanisms. J Clin Oncol 2009; 27: 1235-1242.
[18] Sacks PG, Parnes SM, Gallick GE, Mansouri Z, Lichtner R, Satya-Prakash KL, Pathak S and Parsons DF. Establishment and characterization of two new squamous cell carcinoma cell lines derived from tumors of the head and neck. Cancer Res 1988; 48: 2858-2866.
[19] Gioanni J, Fischel JL, Lambert JC, Demard F, Mazeau C, Zanghellini E, Ettore F, Formento P, Chauvel P, Lalanne CM and et al. Two new human tumor cell lines derived from squamous cell carcinomas of the tongue: establishment, characterization and response to cytotoxic treatment. Eur J Cancer Clin Oncol 1988; 24: 1445-1455.
[20] Thomas SM, Ogagan MJ, Freilino ML, Strychor S, Walsh DR, Gooding WE, Grandis JR and Zamboni WC. Antitumor mechanisms of systemically administered epidermal growth factor receptor antisense oligonucleotides in combination with docetaxel in squamous cell carcinoma of the head and neck. Mol Pharmacol 2008; 73: 627-638.
[21] Barthel H, Cleij MC, Collingridge DR, Hutchinson OC, Osman S, He Q, Luthra SK, Brady F, Price PM and Aboagye EO. 3'-deoxy-3'-[^{18}F]fluorothymidine as a new marker for monitoring tumor response to antiproliferative therapy in vivo with positron emission tomography. Cancer Res 2003; 63: 3791-3798.
[22] Team RDC. R. A language and environment for statistical computing. Vienna, Austria: R Foundation for Statistical Computing, 2009.
[23] Been LB, Suurmeijer AJ, Cobben DC, Jager PL, Hoekstra HJ and Elsinga PH. [^{18}F]FLT-PET in oncology: current status and opportunities. Eur J Nucl Med Mol Imaging 2004; 31: 1659-1672.
[24] Reske SN, Grillenberger KG, Glatting G, Port M, Hildebrandt M, Gansauge F and Beger HG. Overexpression of glucose transporter 1 and increased FDG uptake in pancreatic carcinoma. J Nucl Med 1997; 38: 1344-1348.
[25] Chang PY, Jensen J, Printz RL, Granner DK, Ivy JL and Moller DE. Overexpression of hexokinase II in transgenic mice. Evidence that increased phosphorylation augments muscle glucose uptake. J Biol Chem 1996; 271: 14834-14839.
[26] Mikulits W, Hengstschlager M, Sauer T, Wintersberger E and Mullner EW. Overexpression of thymidine kinase mRNA eliminates cell cycle regulation of thymidine kinase enzyme activity. J Biol Chem 1996; 271: 853-860.
[27] Buck AK, Kratochwil C, Glatting G, Juweid M, Bommer M, Tepsic D, Vogg AT, Mattfeldt T, Neumaier B, Moller P and Reske SN. Early assessment of therapy response in malignant lymphoma with the thymidine analogue [^{18}F]FLT. Eur J Nucl Med Mol Imaging 2007; 34: 1775-1782.
[28] Vesselle H, Grierson J, Muzi M, Pugsley JM, Schmidt RA, Rabinowitz P, Peterson LM, Vallieres E and Wood DE. In vivo validation of 3'deoxy-3'-[(^{18})F]fluorothymidine ([(^{18})F]FLT) as a proliferation imaging tracer in humans: correlation of [(^{18})F]FLT uptake by positron emission tomography with Ki-67 immunohistochemistry and flow cytometry in human lung tumors. Clin Cancer Res 2002; 8: 3315-3323.
[29] Ford AC and Grandis JR. Targeting epidermal growth factor receptor in head and neck cancer. Head Neck 2003; 25: 67-73.
[30] Li M, Ye C, Feng C, Riedel F, Liu X, Zeng Q and Grandis JR. Enhanced antiangiogenic therapy of squamous cell carcinoma by combined endostatin and epidermal growth factor receptor-antisense therapy. Clin Cancer Res 2002; 8: 3570-3578.
[31] Dittmann H, Dohmen BM, Kehlbach R, Bartusek G, Pritzkow M, Sarbia M and Bares R. Early changes in [^{18}F]FLT uptake after chemotherapy: an experimental study. Eur J Nucl Med Mol Imaging 2002; 29: 1462-1469.
[32] Leyton J, Latigo JR, Perumal M, Dhaliwal H, He Q and Aboagye EO. Early detection of tumor re-

sponse to chemotherapy by 3'-deoxy-3'-[^{18}F] fluorothymidine positron emission tomography: the effect of cisplatin on a fibrosarcoma tumor model in vivo. Cancer Res 2005; 65: 4202-4210.

[33] Seol YM, Kwon BR, Song MK, Choi YJ, Shin HJ, Chung JS, Cho GJ, Lee JC, Lee BJ, Wang SG, Kim HJ, Kim WT, Kim SJ and Yun EY. Measurement of tumor volume by PET to evaluate prognosis in patients with head and neck cancer treated by chemo-radiation therapy. Acta Oncol 2010; 49: 201-208.

[34] Hyun SH, Choi JY, Shim YM, Kim K, Lee SJ, Cho YS, Lee JY, Lee KH and Kim BT. Prognostic value of metabolic tumor volume measured by ^{18}F-fluorodeoxyglucose positron emission tomography in patients with esophageal carcinoma. Ann Surg Oncol 2010; 17: 115-122.

[35] Schwartz DL, Rajendran J, Yueh B, Coltrera M, Anzai Y, Krohn K and Eary J. Staging of head and neck squamous cell cancer with extended-field FDG-PET. Arch Otolaryngol Head Neck Surg 2003; 129: 1173-1178.

[36] Fleming AJ Jr, Smith SP Jr, Paul CM, Hall NC, Daly BT, Agrawal A and Schuller DE. Impact of [^{18}F]-2-fluorodeoxyglucose-positron emission tomography/computed tomography on previously untreated head and neck cancer patients. Laryngoscope 2007; 117: 1173-1179.

[37] Gordin A, Golz A, Daitzchman M, Keidar Z, Bar-Shalom R, Kuten A and Israel O. Fluorine-18 fluorodeoxyglucose positron emission tomography/computed tomography imaging in patients with carcinoma of the nasopharynx: diagnostic accuracy and impact on clinical management. Int J Radiat Oncol Biol Phys 2007; 68: 370-376.

[38] Pauwels EK, Sturm EJ, Bombardieri E, Cleton FJ and Stokkel MP. Positron-emission tomography with [^{18}F]fluorodeoxyglucose. Part I. Biochemical uptake mechanism and its implication for clinical studies. J Cancer Res Clin Oncol 2000; 126: 549-559.

[39] Minn H, Clavo AC and Wahl RL. Influence of hypoxia on tracer accumulation in squamous-cell carcinoma: in vitro evaluation for PET imaging. Nucl Med Biol 1996; 23: 941-946.

[40] Bruechner K, Bergmann R, Santiago A, Mosch B, Yaromina A, Hessel F, Hofheinz F, van den Hoff J, Baumann M and Beuthien-Baumann B. Comparison of [^{18}F]FDG uptake and distribution with hypoxia and proliferation in FaDu human squamous cell carcinoma (hSCC) xenografts after single dose irradiation. Int J Radiat Biol 2009; 85: 772-780.

[41] Dence CS, Ponde DE, Welch MJ and Lewis JS. Autoradiographic and small-animal PET comparisons between (^{18})F-FMISO, (^{18})F-FDG, (^{18})F-FLT and the hypoxic selective (^{64})Cu-ATSM in a rodent model of cancer. Nucl Med Biol 2008; 35: 713-720.

[42] Vera P, Bohn P, Edet-Sanson A, Salles A, Hapdey S, Gardin I, Menard JF, Modzelewski R, Thiberville L and Dubray B. Simultaneous positron emission tomography (PET) assessment of metabolism with (1)F-fluoro-2-deoxy-d-glucose (FDG), proliferation with (1)F-fluoro-thymidine (FLT), and hypoxia with (1)fluoro-misonidazole (F-miso) before and during radiotherapy in patients with non-small-cell lung cancer (NSCLC): a pilot study. Radiother Oncol 2011; 98: 109-116.

[43] McGuirt WF, Greven K, Williams D 3rd, Keyes JW Jr, Watson N, Cappellari JO and Geisinger KR. PET scanning in head and neck oncology: a review. Head Neck 1998; 20: 208-215.

[44] Fueger BJ, Czernin J, Hildebrandt I, Tran C, Halpern BS, Stout D, Phelps ME and Weber WA. Impact of animal handling on the results of ^{18}F-FDG PET studies in mice. J Nucl Med 2006; 47: 999-1006.

[45] Dandekar M, Tseng JR and Gambhir SS. Reproducibility of ^{18}F-FDG microPET studies in mouse tumor xenografts. J Nucl Med 2007; 48: 602-607.

[46] Bao A, Phillips WT, Goins B, McGuff HS, Zheng X, Woolley FR, Natarajan M, Santoyo C, Miller FR and Otto RA. Setup and characterization of a human head and neck squamous cell carcinoma xenograft model in nude rats. Otolaryngol Head Neck Surg 2006; 135: 853-857.

[47] Simons AL, Fath MA, Mattson DM, Smith BJ, Walsh SA, Graham MM, Hichwa RD, Buatti JM, Dornfeld K and Spitz DR. Enhanced response of human head and neck cancer xenograft tumors to cisplatin combined with 2-deoxy-D-glucose correlates with increased ^{18}F-FDG uptake as determined by PET imaging. Int J Radiat Oncol Biol Phys 2007; 69: 1222-1230.

[48] Buck AK, Schirrmeister H, Hetzel M, Von Der Heide M, Halter G, Glatting G, Mattfeldt T, Liewald F, Reske SN and Neumaier B. 3-deoxy-3-[(^{18})F]fluorothymidine-positron emission tomography for noninvasive assessment of proliferation in pulmonary nodules. Cancer Res 2002; 62: 3331-3334.

[49] Boothman DA, Davis TW and Sahijdak WM. Enhanced expression of thymidine kinase in human cells following ionizing radiation. Int J Radiat Oncol Biol Phys 1994; 30: 391-398.

[50] Sundseth R, Joyner SS, Moore JT, Dornsife RE and Dev IK. The anti-human immunodeficiency virus agent 3'-fluorothymidine induces DNA damage and apoptosis in human lymphoblastoid cells. Antimicrob Agents Chemother 1996; 40: 331-335.

[51] Atkinson DM, Clarke MJ, Mladek AC, Carlson BL, Trump DP, Jacobson MS, Kemp BJ, Lowe VJ

and Sarkaria JN. Using fluorodeoxythymidine to monitor anti-EGFR inhibitor therapy in squamous cell carcinoma xenografts. Head Neck 2008; 30: 790-799.

[52] Mannheim JG, Judenhofer MS, Schmid A, Tillmanns J, Stiller D, Sossi V and Pichler BJ. Quantification accuracy and partial volume effect in dependence of the attenuation correction of a state-of-the-art small animal PET scanner. Phys Med Biol 2012; 57: 3981-3993.

[53] Ley EJ, Scehnet J, Park R, Schroff S, Dagliyan G, Conti PS, Margulies DR and Salim A. The in vivo effect of propranolol on cerebral perfusion and hypoxia after traumatic brain injury. J Trauma 2009; 66: 154-159; discussion 159-161.

[54] Zheleznyak A, Wadas TJ, Sherman CD, Wilson JM, Kostenuik PJ, Weilbaecher KN and Anderson CJ. Integrin alpha(v)beta (3) as a PET Imaging Biomarker for Osteoclast Number in Mouse Models of Negative and Positive Osteoclast Regulation. Mol Imaging Biol 2012; 14: 500-508.

[55] Grandis JR, Chakraborty A, Melhem MF, Zeng Q and Tweardy DJ. Inhibition of epidermal growth factor receptor gene expression and function decreases proliferation of head and neck squamous carcinoma but not normal mucosal epithelial cells. Oncogene 1997; 15: 409-416.

[56] Agulnik M, da Cunha Santos G, Hedley D, Nicklee T, Dos Reis PP, Ho J, Pond GR, Chen H, Chen S, Shyr Y, Winquist E, Soulieres D, Chen EX, Squire JA, Marrano P, Kamel-Reid S, Dancey J, Siu LL and Tsao MS. Predictive and pharmacodynamic biomarker studies in tumor and skin tissue samples of patients with recurrent or metastatic squamous cell carcinoma of the head and neck treated with erlotinib. J Clin Oncol 2007; 25: 2184-2190.

[57] Soulieres D, Senzer NN, Vokes EE, Hidalgo M, Agarwala SS and Siu LL. Multicenter phase II study of erlotinib, an oral epidermal growth factor receptor tyrosine kinase inhibitor, in patients with recurrent or metastatic squamous cell cancer of the head and neck. J Clin Oncol 2004; 22: 77-85.

[58] Vermorken JB, Trigo J, Hitt R, Koralewski P, Diaz-Rubio E, Rolland F, Knecht R, Amellal N, Schueler A and Baselga J. Open-label, uncontrolled, multicenter phase II study to evaluate the efficacy and toxicity of cetuximab as a single agent in patients with recurrent and/or metastatic squamous cell carcinoma of the head and neck who failed to respond to platinum-based therapy. J Clin Oncol 2007; 25: 2171-2177.

[59] Mishani E, Abourbeh G, Eiblmaier M and Anderson CJ. Imaging of EGFR and EGFR tyrosine kinase overexpression in tumors by nuclear medicine modalities. Curr Pharm Des 2008; 14: 2983-2998.

[60] Mishani E and Hagooly A. Strategies for molecular imaging of epidermal growth factor receptor tyrosine kinase in cancer. J Nucl Med 2009; 50: 1199-1202.

[61] Su H, Seimbille Y, Ferl GZ, Bodenstein C, Fueger B, Kim KJ, Hsu YT, Dubinett SM, Phelps ME, Czernin J and Weber WA. Evaluation of [(^{18})F]gefitinib as a molecular imaging probe for the assessment of the epidermal growth factor receptor status in malignant tumors. Eur J Nucl Med Mol Imaging 2008; 35: 1089-1099.

[62] Yamamoto Y, Nishiyama Y, Ishikawa S, Gotoh M, Bandoh S, Kanaji N, Asakura M and Ohkawa M. 3'-Deoxy-3'-^{18}F-fluorothymidine as a proliferation imaging tracer for diagnosis of lung tumors: comparison with 2-deoxy-2-^{18}F-fluoro-D-glucose. J Comput Assist Tomogr 2008; 32: 432-437.

[63] Yang W, Zhang Y, Fu Z, Yu J, Sun X, Mu D and Han A. Imaging of proliferation with ^{18}F-FLT PET/CT versus ^{18}F-FDG PET/CT in non-small-cell lung cancer. Eur J Nucl Med Mol Imaging 2010; 37: 1291-1299.

[64] Han D, Yu J, Yu Y, Zhang G, Zhong X, Lu J, Yin Y, Fu Z, Mu D, Zhang B, He W, Huo Z, Liu X, Kong L, Zhao S and Sun X. Comparison of (^{18})F-fluorothymidine and (^{18})F-fluorodeoxyglucose PET/CT in delineating gross tumor volume by optimal threshold in patients with squamous cell carcinoma of thoracic esophagus. Int J Radiat Oncol Biol Phys 2010; 76: 1235-1241.

[65] van Westreenen HL, Cobben DC, Jager PL, van Dullemen HM, Wesseling J, Elsinga PH and Plukker JT. Comparison of ^{18}F-FLT PET and ^{18}F-FDG PET in esophageal cancer. J Nucl Med 2005; 46: 400-404.

[66] Linecker A, Kermer C, Sulzbacher I, Angelberger P, Kletter K, Dudczak R, Ewers R and Becherer A. Uptake of (^{18})F-FLT and (^{18})F-FDG in primary head and neck cancer correlates with survival. Nuklearmedizin 2008; 47: 80-85; quiz N12.

[67] Yang H, Berger F, Tran C, Gambhir SS and Sawyers CL. MicroPET imaging of prostate cancer in LNCAP-SR39TK-GFP mouse xenografts. Prostate 2003; 55: 39-47.

[68] Zhang Y, Saylor M, Wen S, Silva MD, Rolfe M, Bolen J, Muir C, Reimer C and Chandra S. Longitudinally quantitative 2-deoxy-2-[^{18}F]fluoro-D-glucose micro positron emission tomography imaging for efficacy of new anticancer drugs: a case study with bortezomib in prostate cancer murine model. Mol Imaging Biol 2006; 8: 300-308.

[69] Nanni C, Di Leo K, Tonelli R, Pettinato C, Rubello D, Spinelli A, Trespidi S, Ambrosini V, Cas-

tellucci P, Farsad M, Franchi R, Pession A and Fanti S. FDG small animal PET permits early detection of malignant cells in a xenograft murine model. Eur J Nucl Med Mol Imaging 2007; 34: 755-762.

[70] Jost SC, Wanebo JE, Song SK, Chicoine MR, Rich KM, Woolsey TA, Lewis JS, Mach RH, Xu J and Garbow JR. In vivo imaging in a murine model of glioblastoma. Neurosurgery 2007; 60: 360-370; discussion 370-361.

[71] Solit DB, Santos E, Pratilas CA, Lobo J, Moroz M, Cai S, Blasberg R, Sebolt-Leopold J, Larson S and Rosen N. 3'-deoxy-3'-[^{18}F]fluorothymidine positron emission tomography is a sensitive method for imaging the response of BRAF-dependent tumors to MEK inhibition. Cancer Res 2007; 67: 11463-11469.

[72] Tseng JR, Kang KW, Dandekar M, Yaghoubi S, Lee JH, Christensen JG, Muir S, Vincent PW, Michaud NR and Gambhir SS. Preclinical efficacy of the c-Met inhibitor CE-355621 in a U87 MG mouse xenograft model evaluated by ^{18}F-FDG small-animal PET. J Nucl Med 2008; 49: 129-134.

[73] Ma WW, Jacene H, Song D, Vilardell F, Messersmith WA, Laheru D, Wahl R, Endres C, Jimeno A, Pomper MG and Hidalgo M. [^{18}F]fluorodeoxyglucose positron emission tomography correlates with Akt pathway activity but is not predictive of clinical outcome during mTOR inhibitor therapy. J Clin Oncol 2009; 27: 2697-2704.

[74] von Forstner C, Egberts JH, Ammerpohl O, Niedzielska D, Buchert R, Mikecz P, Schumacher U, Peldschus K, Adam G, Pilarsky C, Grutzmann R, Kalthoff H, Henze E and Brenner W. Gene expression patterns and tumor uptake of ^{18}F-FDG, ^{18}F-FLT, and ^{18}F-FEC in PET/MRI of an orthotopic mouse xenotransplantation model of pancreatic cancer. J Nucl Med 2008; 49: 1362-1370.

[75] Shah C, Miller TW, Wyatt SK, McKinley ET, Olivares MG, Sanchez V, Nolting DD, Buck JR, Zhao P, Ansari MS, Baldwin RM, Gore JC, Schiff R, Arteaga CL and Manning HC. Imaging biomarkers predict response to anti-HER2 (ErbB2) therapy in preclinical models of breast cancer. Clin Cancer Res 2009; 15: 4712-4721.

[76] Debucquoy A, Devos E, Vermaelen P, Landuyt W, De Weer S, Van Den Heuvel F and Haustermans K. ^{18}F-FLT and ^{18}F-FDG PET to measure response to radiotherapy combined with celecoxib in two colorectal xenograft models. Int J Radiat Biol 2009; 85: 763-771.

[77] Honer M, Ebenhan T, Allegrini PR, Ametamey SM, Becquet M, Cannet C, Lane HA, O'Reilly TM, Schubiger PA, Sticker-Jantscheff M, Stumm M and McSheehy PM. Anti-Angiogenic/Vascular Effects of the mTOR Inhibitor Everolimus Are Not Detectable by FDG/FLT-PET. Transl Oncol 2010; 3: 264-275.

[78] Brepoels L, De Saint-Hubert M, Stroobants S, Verhoef G, Balzarini J, Mortelmans L and Mottaghy FM. Dose-response relationship in cyclophosphamide-treated B-cell lymphoma xenografts monitored with [^{18}F]FDG PET. Eur J Nucl Med Mol Imaging 2010; 37: 1688-1695.

[79] Revheim ME, Roe K, Bruland OS, Bach-Gansmo T, Skretting A and Seierstad T. Monitoring the Effect of Targeted Therapies in a Gastrointestinal Stromal Tumor Xenograft Using a Clinical PET/CT. Mol Imaging Biol 2010.

[80] Caretti V, Zondervan I, Meijer DH, Idema S, Vos W, Hamans B, Bugiani M, Hulleman E, Wesseling P, Vandertop WP, Noske DP, Kaspers G, Molthoff CF and Wurdinger T. Monitoring of tumor growth and post-irradiation recurrence in a diffuse intrinsic pontine glioma mouse model. Brain Pathol 2011; 21: 441-451.

[81] Valentiner U, Haane C, Peldschus K, Gustke H, Brenner W, Wilke F, Pommert A, Owsijewitsch M, Schumacher U and Klutmann S. [^{18}F]FDG and [^{18}F]FLT PET-CT and MR imaging of human neuroblastomas in a SCID mouse xenograft model. Anticancer Res 2008; 28: 2561-2568.

[82] Sun X, Yan Y, Liu S, Cao Q, Yang M, Neamati N, Shen B, Niu G and Chen X. ^{18}F-FPPRGD2 and ^{18}F-FDG PET of response to Abraxane therapy. J Nucl Med 2011; 52: 140-146.